Robust Windowed Harmonic Phase Analysis with a Single Acquisition

Santiago Sanz-Estébanez[1], Lucilio Cordero-Grande[2], Marcos Martín-Fernández[1], and Carlos Alberola-López[1]

[1] Laboratorio de Procesado de Imagen, Universidad de Valladolid, España
ssanest@lpi.tel.uva.es, {marcma, caralb}@tel.uva.es,
[2] Biomedical Engineering Department, King's College, London, U.K.
lucilio.cordero_grande@kcl.ac.uk

Abstract. The HARP methodology is a widely extended procedure for cardiac tagged magnetic resonance imaging since it is able to analyse local mechanical behaviour of the heart; extensions and improvements of this method have also been reported since HARP was released. Acquisition of an over-determined set of orientations is one of such alternatives, which has notably increased HARP robustness at the price of increasing examination time. In this paper, we explore an alternative to this method based on the use of multiple peaks as opposed to multiple orientations, intended for a single acquisition. Performance loss is explored with respect to multiple orientations in a real setting. In addition, we have assessed, by means of a computational phantom, optimal tag orientations and spacings of the stripe pattern by minimizing the Frobenius norm of the difference between the ground truth and the estimated material deformation gradient tensor. Results indicate that, for a single acquisition, multiple peaks as opposed to multiple orientations, are indeed preferable.

Keywords: Cardiac Tagged Magnetic Resonance Imaging; Harmonic Phase; Multi-Harmonic Analysis; Robust Strain Reconstruction

1 Introduction

Measures of local myocardial deformation are essential for a deeper comprehension of heart functionalities for both normal and pathologic subjects [1]. Tagged magnetic resonance (MR-T) is a noninvasive method for assessing the displacement of heart tissue over time [2]. This modality is based on the generation of a set of saturated magnetization planes on the imaged volume, so that material points may be tracked throughout the cardiac cycle [3] and local functional indicators, such as the strain tensor [4], can be estimated.

Regarding the analysis of MR-T images [5], we can differentiate two main families of methods, image-based and k-space-based techniques. The image-based techniques are devised to directly process and analyse the tagged images by identifying the tag lines and tracking their deformation between frames. Examples of such techniques are optical flow [6] or deformable models [7] methodologies.

Alternatively, the k-space-based approaches rely on the Fourier Transform (FT) of the tagged images. Compared to the image-based, k-space-based techniques have proven to be much faster and less prone to artifacts [8]. Most notable methodologies in this category are sine wave modeling (SinMod) [9] and HARmonic Phase (HARP) [10] analysis. Recent studies have reported that, although both techniques are consistent in motion estimates, an exaggeration in measurements is often observed for SinMod [8], leading to larger biases. Therefore, we have focused on HARP-based methods. These methods are grounded on the extraction of the complex image phase obtained by band-pass (BP) filtering the spectral peaks introduced by the applied modulation; they rely on the fact that the extracted harmonic phase is linearly related to a directional component of the true motion [10]. Hence, dense displacement fields can be recovered on the basis on a constant local phase assumption, which turns out to be more reliable than a constant pixel brightness assumption.

An in-depth study of the HARP method is provided in [11]; the author uses a communications-based approach to analyze the method in detail, including resolution, dynamic range and noise. Signal processing solutions based on the Windowed Fourier Transform (WFT) [12] have been proposed to balance the spatial and spectral localization of the image, thus obtaining smooth local phase estimations. Adaptive approaches have been subsequently proposed in [13, 14] in order to accommodate tag local properties both in window and filter designs, respectively. However, slight improvements have been reported with respect to non-adaptive methods, taking into account the considerable computational cost increasing.

Techniques to synthesize more desirable tag patterns have also been proposed using multiple harmonic peaks, both with different tag spacings [15] and new profiles [16]. Methodologies that make use of multiple orientations [17–19] have also been devised to improve the quality of the estimated motion at the prize of increasing acquisition time. Besides, these methodologies require of non-trivial image registration techniques to align the multiple acquisitions, which itself may also have an important impact on processing conclusions.

In this paper we depart from the reported idea that using an overdetermined set of orientations (MO) significantly increases the quality of the estimated deformation gradient tensor [19]; however, our purpose is to convey information within a single acquisition at the expense of a worse performance with respect to multiple acquisitions. Therefore, we have explored performance of using two peaks with two orthogonal orientations within a single acquisition, as opposed to multiple single-peaked orientations in multiple acquisitions, and we quantify performance loss. Then, we find out by optimization both tag orientation and spacing of two stripes patterns that are set free when another two are set beforehand. Interestingly, our results show that the latter approach converges to the former, i.e., two orthogonal orientations with two peaks is the preferable solution when a unique acquisition is pursued.

2 Materials

MR-T is usually performed by SPAtial Modulation of Magnetization (SPAMM) [20], which is grounded on the ability of altering the magnetization of the tissue in presence of motion. This process will generate a modulation with different sinusoidal functions. Each of these sinusoids will be given by its wave vector $\mathbf{k}_i$ with $\mathbf{k}_i = k_i \mathbf{u}_i$, where k_i is the wave number (related to its frequency) and $\mathbf{u}_i$ its orientation vector (corresponding to the orientation of the applied gradient).

We have acquired a medial slice on an adult volunteer using a MR SPAMM SENSitivity Encoding (SENSE) Turbo Field Echo sequence on a Philips Achieva 3T scanner. The image has a spatial resolution of $1.333 \times 1.333\,\mathrm{mm}^2$ and a slice thickness of 8 mm. The acquisition parameters are $T_E = 3.634\,\mathrm{ms}$, $T_R = 6.018\,\mathrm{ms}$ and $\alpha = 10°$. Regarding the tagging parameters, the tag spacing has been set to $\lambda = 7\,\mathrm{mm}$, with its different harmonic peaks at $\mathbf{k} = \{1, 2\}/\lambda$ and different orientations $u_i = (\cos(\theta_i), \sin(\theta_i))$. The specific orientations are $\theta_i = -85° + i \cdot 5°$ with $0 \le i \le 35$, therefore with $-85° \le \theta_i \le 90°$. Two grid patterns have also been acquired with $\{45°\text{- } 135°\}$ and $\{0°\text{- } 90°\}$ orientations.

Simulated SPAMM sequences [21] have also been launched both with one (1D) and two orientations (2D) with different λ values and multiple spectral peaks, some examples of which are shown in Fig. 1. Harmonic coefficients have been set according to [16].

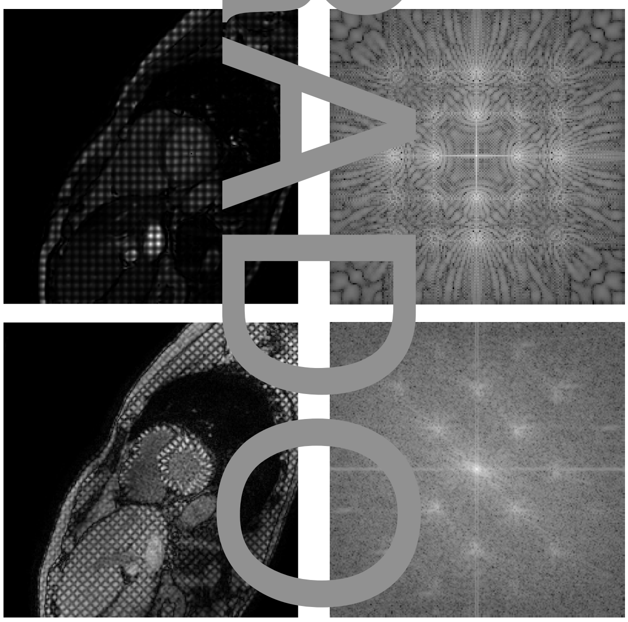

Fig. 1. The two upper images show synthetic data (2D) while real dataset is sketched below for 2D in a $\{45°\text{- } 135°\}$ grid. All intermodulations for the 2D case are present.

Optimization experiments have been [illegible]ned on the synthetic data; the computational phantom consists in an annulus centered at the myocardium with $R_i = 28$ and $R_o = 40$ as its inner and its outer radii, respectively. An incompressible radially varying deformation has also been applied according to $r = \sqrt{R^2 - \gamma R_i^2}$, where γ controls the degree of deformation and r and R represent the spatial and material radial coordinates, respectively. Notice that for the simulated SPAMM synthetic data, we have not included noise, tag fading or other undesired effects. We have preferred not to simulate these confounding factors, which are present in real data, in order to remove its influence in the final tag pattern design.

3 Method

3.1 Reconstruction Pipeline

As stated in [10], HARP motion reconstruction using SPAMM requires a minimum of 2 linearly independent wave vectors. The proposed approach allows us to accommodate multiple wave vectors stemming from the different orientations and harmonic peaks. Reconstruction pipeline can be summarized in the following steps (see Fig. 2):

- **Calculation of the local phase of the image.** For a given cardiac phase, we compute the 2D discrete WFT [illegible] to obtain the local spectrum $S[\mathbf{m}]$ for each image $I[\mathbf{x}]$. The window employed at this step is real, even, of unit norm, and monotonically decreasing for positive values of its argument. Hence, the obtained discrete WFT can be seen as a set of discrete FTs applied to the result of windowing an image throughout its support.
  Once local spectrum is calculated, a complex BP filter is applied to extract the corresponding phase to each wave vector i. Therefore, for each pixel of the image, we have built a circumferential spectral filter, whose radius is linearly related to a previously defined bandwidth, which has been centered at the maximum of the spectra inside a predefined region located in the surroundings of the reference spatial frequency of the tags.
  The final WHARP image, for each wave vector, can be reconstructed in the spatial domain by using an inverse WFT (IWFT) from which its phase is readily extracted, i.e., $\phi_i[\mathbf{x}] = \angle \hat{I}_i[\mathbf{x}]$.
- **Material deformation gradient tensor estimation at end-systolic phase.** The material deformation gradient tensor $\mathbf{F}(\mathbf{x})$ can be estimated from the gradient of the phase image $\mathbf{Y}(\mathbf{x})$ as stated in [10]. Robust estimation of $\mathbf{F}(\mathbf{x})$ is achieved through Least Absolute Deviation (LAD) procedure [22]. Reconstruction is performed via Iteratively Reweighted Least Squares:

$$\mathbf{F}_{l+1}(\mathbf{x}) = (\mathbf{Y}^T(\mathbf{x})\mathbf{W}_l(\mathbf{x})\mathbf{Y}(\mathbf{x}))^{-1}\mathbf{Y}^T(\mathbf{x})\mathbf{W}_l(\mathbf{x})\mathbf{K}, \tag{1}$$

  where $\mathbf{K}$ represents the given wave vectors and $\mathbf{W}_l(\mathbf{x})$ a diagonal weighting matrix updated at each itera[illegible]ng the fitting residuals [19]. For illustration purposes, the Green-Lagrange strain tensor is also computed in the polar coordinate system.

3.2 Optimal Tag Pattern S[illegible]

In order to find the optimal tag pattern, we have carried out an optimization procedure on the synthetic data; the procedure is schematically shown in Fig. 2. The upper part shows how the ground-truth data is obtained. First, the stripe patterns, consisting in two sets of two orthogonal directions are generated. Each pattern is then applied to a previously acquired cine sequence. Each pattern is applied in isolation so that no interference arises. Then, the methodology described in Section. 3.1 is applied to calculate F^{GT}.

The stripes are oriented as $\{0°, 45°, 90°, 135°\}$ with $\lambda = 7.15$ mm and only the DC component and the two symmetric peaks are included in the simulation. The analysis window w of the WFT is defined as stated in Section 3.1 and its size has been set to $\mathbf{Q} = [32, 32]$.

The BP filter parameters, for each pixel $\mathbf{x}$ and wave vector i, are represented as $\boldsymbol{\beta}_i[\mathbf{x}] = (\hat{\mathbf{k}}_i[\mathbf{x}], \rho)$, where ρ is the radius of the filter, which is centered at $\hat{\mathbf{k}}[\mathbf{x}]$.The filter bandwidth is normalized with respect to the wave number ($\mu = \rho/k$, $k = 2\pi/\lambda$) so that area of all filters remains the same along the pipeline.

As for the lower part of the figure, the tags are multiplied to each other as well as to the cine sequence; intermodulations are therefore present in the problem. Then, the aforementioned reconstruction procedure is performed but for the fact that the WFT is applied to the image degraded by interference. When the BP filter bank is applied, channels are processed in parallel. In this case, two stripes ($\{0°, 90°\}$) remain fixed with the tag spacing at $\lambda_{1,2} = 7.15$ mm. The other two stripes are considered as variables in the optimization problem, both in tag orientation and spacing $(\theta_3, \theta_4, \lambda_3, \lambda_4)$. The objective function to be minimized is defined upon the Frobenius Norm Difference (FND) between a ground-truth tensor F^{GT} and the estimated tensor with a specific value of the variable $\boldsymbol{\Theta}$ (see below); this function is integrated over a predefined region of interest χ that encloses the myocardium. Formally:

$$\boldsymbol{\Theta}^* = \arg\min_{\boldsymbol{\Theta}} \int_\chi FND(\mathbf{x}, \boldsymbol{\Theta})^2 d\chi = \arg\min_{\boldsymbol{\Theta}} \int_\chi \sum_{m=1}^{2} \sum_{n=1}^{2} (F_{mn}^{GT}(\mathbf{x}) - F_{mn}(\mathbf{x}, \boldsymbol{\Theta}))^2 d\chi$$

with $\boldsymbol{\Theta} = \left[\theta_3, \theta_4, \lambda_3, \lambda_4\right]$.

The solution has been obtained [illegible] the Nelder-Mead algorithm [23]. This algorithm does not require derivatives of the objective function. Simulation has been limited to four stripes to [illegible] overwhelming peak interference.

4 Evaluation and Discussion

The importance of the number of [illegible] is measured in Fig. 3 in terms of reproducibility for the real dataset. Estimated tensors should be equal irrespective of the stripe pattern used; [illegible] measure of reproducibility is the FND defined above but applied in this case to two instances of the reconstructed tensor with two different, albeit comparable, stripe sets. Specifically,

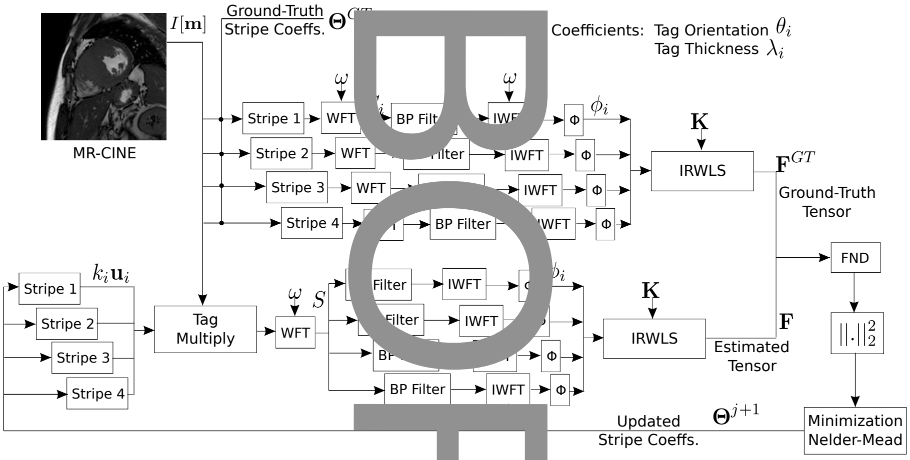

Fig. 2. Flowchart of the optimization procedure for optimal stripes parameter search. Notice that connections from the Nelder-Mead algorithm to stripes 1 and 2 do not undergo any variation.

given two stripe sets with the same number of orientations and their respective reconstructed tensors, we have calculated the median of the $FND(\mathbf{x})$ with both for $\mathbf{x} \in \chi$.

Fig. 3 shows the impact on reproducibility of using either additional orientations or additional harmonic peaks.

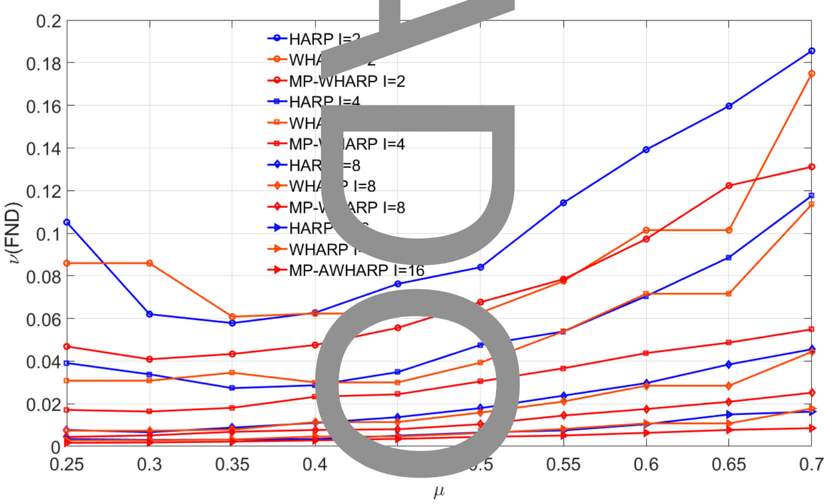

Fig. 3. Median of the FND $\forall \mathbf{x} \in \chi$ obtained with different number of images as a function of the filter bandwidth μ.

As previously described [19], a combined set of stripes increases reproducibility at the price of a higher number of acquisitions. For a given number of orientations the multi-peak (MP) windowed approach (WHARP) shows additional improvement for moderate bandwidth. HARP analysis has also been added showing lower figures. When bandwidth is excessive, interference from nearby peaks reduces the stability of results. MP-WHARP obtained with I=2 is located halfway between the other results with I=2 and those with I=4. This solution would require a single acquisition while I=4 requires at least two, for a grid pattern.

For the synthetic dataset, Fig. 4 shows the mean squared error (MSE) of the strain tensor principal components ($\hat{E}^{rr}$) and ($\hat{E}^{cc}$) for different options (windowed, MP, MO) as a function of the degree of deformation γ. In these figures solid lines are obtained with multiple images (I=18) and dashed lines with only two orthogonal directions (I=1); in both, grid patterns have been used. As can be observed, MO and MP play a satisfactory role for moderate values of γ. It is worthy to say that MP approach presents a notable performance, even with a unique grid-like acquisition. On the other side, when severe deformation is applied to the I=1 cases, non-MP approaches depart dramatically from the ground truth while LAD algorithm maintains quality fairly unaltered for the MP version (dashed-red line).

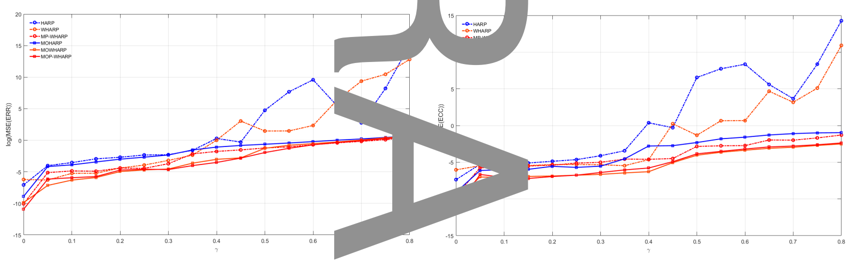

Fig. 4. Log-mean squared error of ($\hat{E}^{rr}$) (left) and ($\hat{E}^{cc}$) (right) for $\mu = 0.35$. Solid line denotes reconstruction error with 18 images while dashed dashed lines are obtained with only two.

In Fig. 5, we show the output of the optimization procedure described in Section. 3.2. According to the figure, the two free orientations turn out to align with the two that remained fixed, although spectral separation is lower than the separation of the steady peaks with respect to the DC component; specifically, the steady peaks are located at $k = 7.15^{-1} = 0.14$ mm^{-1}, while the other two turn out to be located (on average) $k \sim \frac{1.6}{7.15}$ mm^{-1}. This output, however, is not directly available in equipments currently used in clinical settings.

Therefore, we have carried out an additional two-fold experiment in order to test relevance of peak separation or, equivalently, tag spacing. For this purpose, we have calculated the MSE in E^{rr} estimation for both 1D and 2D cases; for the former, we have simulated a pattern with two peaks in the same direction, where

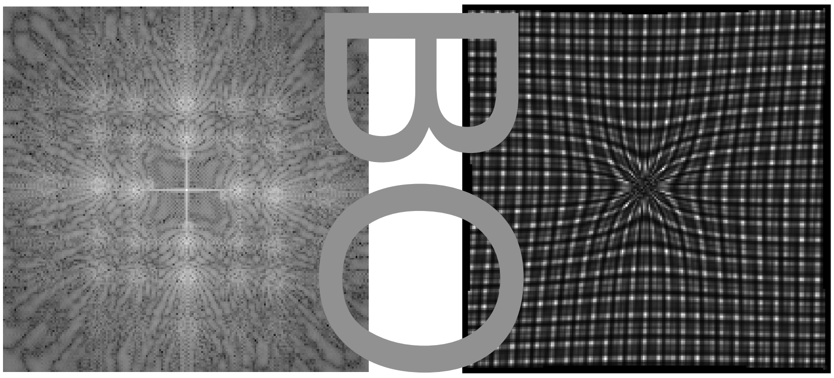

Fig. 5. Final configuration of the [illegible]ned with Nelder-Mead algorithm both on k-space (left figure) and spatial domain (centered at right figure) with $\gamma = 0.45$.

the first peak is located at λ_1 = [illegible] and [illegible] second peak is translated, in k-space, along that direction. For the latter, the pattern consists of a multiplication of two such 1D patterns in orthogonal directions. Results, as shown in Fig. 6, indicate that optimal separation depends on the degree of deformation γ, with higher sensitivity in the 1D case, whereas, for 2D, sensitivity is much lower for $\gamma \geq 0.3$. In this interval, performance is fairly constant so a $\frac{1}{\lambda_1} = 0.14$ separation, i.e., location of harmonically rel[illegible]ns an appropriate design choice. This is the case of a grid pattern with second order SPAMM acquisition, which is a commonly available sequence. Presence of noise and tag fading in simulation will presumably increase smearing in k-space, making this space more crowded, so this conclusions tend to reinforce. With this in mind, it may be appealing to include even more peaks in the acquisition. However, growing between-peak-interference may severely affect estimates. For that reason, we have limited our experiments to a maximum of four stripes per acquired image. Further research should be developed in this dir[illegible] the influence of heavily-peaked acquisitions in the robustness of reconstruction[illegible]

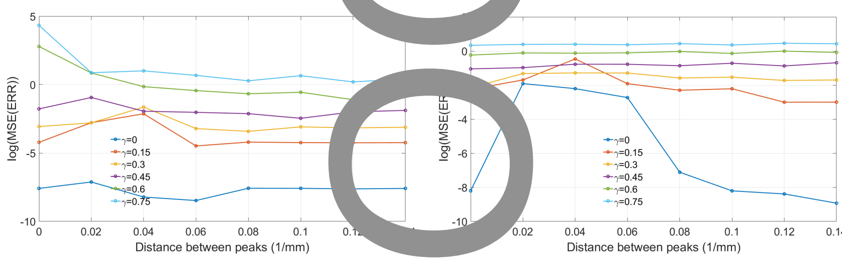

Fig. 6. Log-mean squared error in [illegible] a function of the distance between peaks in presence of different degrees of deformation with a fixed $\mu = 0.35$. 1D and 2D cases have been plotted in left and right figures, respectively

Additionally, in Fig. 7 we sho[illegible]ined on real data with different stripe sets for different bandwidths; we have used as a silver estimate of **F** the one obtained with the eight 1D orientations indicated in Section. 2. Specifically, we have tried the following subsets: {45°- 135°} and {0°- 90°} in a grid (2D) pattern with two peaks per orientation, and {45°- 135°}, {0°- 90°}, {45°- 135°- 0°- 90°} and {30°- 60°- 120°- 150°} for line (1D) acquisitions with a unique peak. The figure reveals that harmonic MP solution with a single acquisition overcomes the solution obtained with two orthogonal line acquisitions and it provides a reasonable performance loss with respect to four orientation reconstructions, i.e., those needing two acquisitions, at least, in commercial equipments. Therefore, we can conclude that our solution sho[illegible] an appropriate balance between estimation robustness and time consumption.

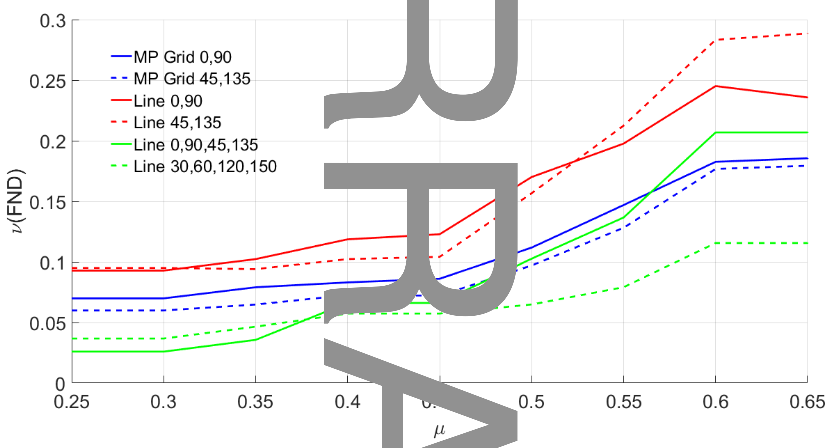

Fig. 7. Median of the FND obta[illegible] with different stripe sets as a function of μ.

Finally, in Fig. 8 we show $E^{r[illegible]}$ and E^{cc} estimates from the simulated SPAMM data using the different methods (FT, WFT and MP-WFT) using two grid images for the FT and WFT approaches, while only one has been employed for the proposed MP-WFT approach ([illegible] vectors in total).

Visual results illustrate about the influence of bandwidth; when using smaller ones strain is underestimated wh[illegible] incrementing significant artifacts and interferences arise. Obviously, the emergence of these artifacts would be greatly limited by the use of a larger number of wave vectors, although MP-WFT approach seems less prone to them.

5 Conclusions

In this paper we have described a robust alternative to the original HARP method, intended for a single acquisition. To this end, we have observed that in-

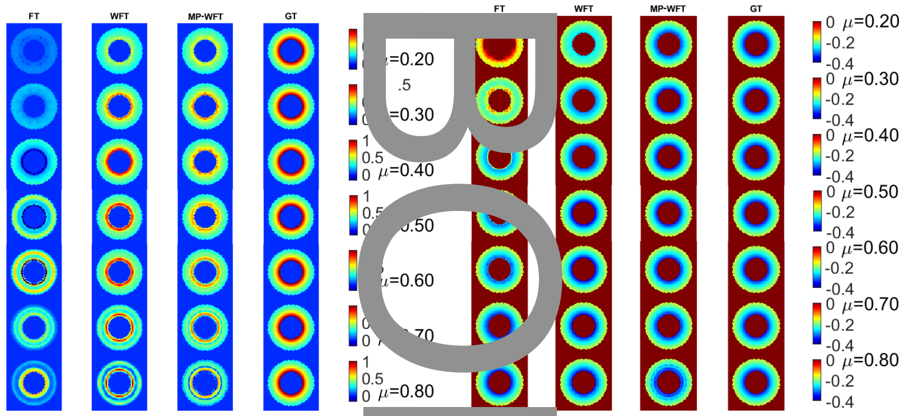

Fig. 8. E^{rr} (left) and E^{cc} (right) strain components for synthetic data obtained for different bandwidths and methodologies. Ground-truth (GT) is also shown for the sake of comparison.

formation comprised by various [illegible] e pattern is useful for achieving robust results despite using a unique acquisition. We have quantified performance of this solution with respect to multi-oriented solutions.

Simulation results indicate that four orientations converge into an orthogonal grid with harmonically related peaks ([illegible] mid to high deformation degree interval) for an optimal performance, so multiple peaks as opposed to multiple stripes is a preferable solution. The proposed pattern has also shown comparable results, for the case of a single acquisition, to those obtained with two different grid acquisitions, while the latter doubles the scan time.

Furthermore, the proposed multi-[illegible] method has significantly improved both the accuracy and the reproducibility of strain measurements with respect to the standard acquisition in which just two orthogonal orientations are acquired, using same amount of time. With the proposed design, current acquisition protocols can be easily recast to include multiple peaks, which could simultaneously improve the resolution, robustness and precision of motion sensitive MR imaging and its subsequent analysis.

Acknowledgments. This work was partially supported by the European Regional Development Fund (ERDF-FEDER) under Research Grants TEC2014-57428-R and TEC2017-82408-R and the Spanish Junta de Castilla y León under Grant VA069U16.

References

1. Jeung, M., Germain, P., Croisille, P., [illegible]udi, S., Roy, C., Gangi, A.: Myocardial Tagging with MR Imaging: Overview of Normal and Pathologic Findings. RadioGraphics 32, 1381–1398 (2012)

2. Shehata, M., Cheng, S., Osman, N., Bluemke, D., Lima, J.: Myocardial Tissue Tagging with Cardiovascular Magnetic Resonance. J Cardiovasc Magn Reson 11(1), 55 (2009)
3. Ibrahim, E.: Myocardial Tagging by Cardiovascular Magnetic Resonance: Evolution of Techniques Pulse Sequences, Analysis, Algorithms and Applications. J Cardiovasc Magn Reson 13, 36 (2011)
4. Simpson, R., Keegan, J., Firmin, D.: MR Assessment of Regional Myocardial Mechanics. J Cardiovasc Magn Reson 37, 576–599 (2013)
5. Axel, L., Montillo, A., Kim, D.: Tagged Magnetic Resonance Imaging of the Heart: a Survey. Med Image Anal 9, 376–393 (2005)
6. Horn, B., Schunck, B.: Determining optical flow. Artificial Intel 17, 185–203 (1981)
7. Young, A., Axel, L.: Three-dimensional Motion and Deformation of the Heart Wall: Estimation with Spatial Modulation of Magnetization-A Model-based Approach. Radiology 185(1), 241–247 (1992)
8. Ibrahim, E., Swanson, S., Stojanovska, J., Duvernoy, C., Pop-Busui, R.: Harmonic Phase Versus Sine-Wave Modulation for Measuring Regional Heart Function from Tagged MRI Images. In: 13th IEEE ISBI. Prague, Czech Republic (2016)
9. Arts, T., Prinzen, F., Delhaas, T., Milles, J., Rossi, A., Clarysse, P.: Mapping displacement and deformation of the heart with local sine-wave modeling. Trans Med Imag 29, 1114–23 (2010)
10. Osman, N., McVeigh, E., Prince, J.: Imaging Heart Motion using Harmonic Phase MRI. IEEE Trans Med Imaging 19(3), 186–202 (2000)
11. Parthasarathy, V.: Characterization of Harmonic Phase MRI: Theory, Simulations and Applications. Ph.D. thesis, Doctoral dissertation, Johns Hopkins University (2006)
12. Cordero-Grande, L., Vegas-Sánchez-Ferrero, G., Casaseca-de-la-Higuera, P., Alberola-López, C.: Improving harmonic phase imaging by the windowed Fourier transform. In: 8th IEEE International Symposium on Biomedical Imaging: From Nano to Macro. pp. 520–523. Chicago, USA (March-April 2011)
13. Fu, Y., Chui, C., Teo, C.: Accurate two-dimensional Cardiac Strain Calculation using Adaptive Windowed Fourier Transform and Gabor Wavelet Transform. Int J Comput Assist Radiol Surg 8(1), 135–144 (2013)
14. Sanz-Estébanez, S., Cordero-Grande, L., Martín-Fernández, M., Aja-Fernández, S., Alberola-López, C.: Spatia[illegible] Anisotropy in HARP Images: An Automated Approach. In: IEEE International Symposium on Biomedical Imaging: From Nano to Macro. pp. 1105–1108. Prague, Czech Republic (2016)
15. Atalar, E., McVeigh, E.: Optimization of Tag Thickness for Measuring Position with Magnetic Resonance Imaging. IEEE Trans Med Imag 13(1), 152–160 (1994)
16. Osman, N., Prince, J.: Regenerating MR Tagged Images Using Harmonic Phase (HARP) Methods. IEEE Trans Biomed Eng 51(8), 1428–1433 (2004)
17. Mosher, T., Smith, M.: A DANTE Tagging Sequence for the Evaluation of Translational Sample Motion. Magn Reson Med 15, 334–339 (1990)
18. Agarwal, H., Prince, J., Abd-Elmoniem, K.: Total Removal of Unwanted Harmonic Peaks (TruHARP) MRI for Single Breath-Hold High-Resolution Myocardial Motion and Strain Quantification. Magn Reson Med 64(2), 574–585 (2010)
19. Cordero-Grande, L., Royuela-del-Val, J., Sanz-Estébanez, S., Martín-Fernández, M., Alberola-López, C.: Multi-Oriented Windowed Harmonic Phase Reconstruction for Robust Cardiac Strain Imaging. Med Image Anal 29, 1–11 (2016)
20. Axel, L., Dougherty, L.: MR Imaging of Motion with Spatial Modulation of Magnetization. Radiology 171(3), 841–845 (1989)

21. Rutz, A., Ryf, S., Plein, S., Boesiger, P., Kozerke, S.: Accelerated Whole-Heart 3D CSPAMM for Myocardial Motion Quantification. Magn Reson Med 59, 755–763 (2008)
22. Cordero-Grande, L., Royuela-del-Val, J., Martín-Fernández, M., Alberola-López, C.: MOWHARP: Multi-oriented Windowed HARP Reconstruction for Robust Strain Imaging. In: 22nd Proceedings of the International Society on Magnetic Resonance in Medicine. p. 7540. Milan, Italy (May 2014)
23. Nelder, J., Mead, R.: A Simplex Method for Function Minimization. Computer Journ 7, 308–313 (1965)